

## The H-mode threshold in JET with the ITER-like wall

C.F. Maggi<sup>1</sup>, G. Calabro<sup>2</sup>, E. Delabie<sup>3</sup>, M. Groth<sup>4</sup>, N.C. Hawkes<sup>5</sup>, M. Lehnen<sup>6</sup>,  
E. de la Luna<sup>7</sup>, K. McCormick<sup>1</sup>, F. Militello<sup>5</sup>, C. Reux<sup>8</sup>, F. Rimini<sup>5</sup>, E.R. Solano<sup>7</sup>,  
V. Bobkov<sup>1</sup>, M. Brix<sup>5</sup>, A. Czarnecka<sup>9</sup>, J. Flanagan<sup>5</sup>, E. Lerche<sup>10</sup>, S. Marsen<sup>11</sup>, I. Nunes<sup>12</sup>,  
B. Sieglin<sup>1</sup>, D. Van Eester<sup>10</sup> and JET EFDA Contributors\*

*JET-EFDA, Culham Science Centre, Abingdon, OX14 3DB, UK*

<sup>1</sup>MPI für Plasmaphysik, EURATOM Association, D-85748 Garching, Germany; <sup>2</sup>Associazione EURATOM-ENEA, Frascati, Italy; <sup>3</sup>Association EURATOM-FOM, Nieuwegein, The Netherlands; <sup>4</sup>Aalto University, Association EURATOM-Tekes, 02015 Espo, Finland; <sup>5</sup>CCFE Fusion Association, Abingdon, OX14 3DB, UK; <sup>6</sup>Association EURATOM-FZ, Jülich, Germany; <sup>7</sup>Asociacion EURATOM-CIEMAT, Madrid, Spain; <sup>8</sup>Association EURATOM CEA, St Paul lez Durance, France; <sup>9</sup>Association EURATOM-IPPLM, Poland; <sup>10</sup>LPP-ERM/KMS EURATOM Association, Belgium; <sup>11</sup>MPI für Plasmaphysik, EURATOM Association, D-17491 Greifswald, Germany; <sup>12</sup>Associacao EURATOM-IST, Lisboa, Portugal

\*See App. of F. Romanelli et al., Proc. of the 23rd IAEA Fusion Energy Conf. 2010, Daejeon, Korea

**1. Introduction.** In preparation for ITER, JET's main plasma facing components, previously of carbon, have been replaced with a new ITER-like wall (ILW), with mainly Be in the main chamber and W in the divertor. This paper reports on recent JET studies on the influence of the ILW on the H-mode power threshold,  $P_{\text{thr}}$ , at low plasma density ( $n_e$ ), in particular with respect to modifications in the radiated power compared to the C wall. This is of value to ITER, whose predicted  $P_{\text{thr}}$  is extrapolated from scaling laws of the loss power,  $P_{\text{loss}}$ , with no account for radiation [1].

**2. L-H transitions at low density with C wall.** While the scaling law for the power threshold,  $P_{\text{thr},08} \sim n_e^{0.717} B_T^{0.803} S^{0.94}$ , is only valid for medium to high densities, many tokamak experiments have observed an increase of  $P_{\text{thr}}$  and edge  $T_e$  with decreasing  $n_e$ , below a minimum density,  $n_{e,\text{min}}$  [1]. In JET, this was first observed with the MkII-GB divertor [2], [3]. However, after removal of the divertor septum (MkII-GB SRP) [3] and, more recently, with the current MkII-HD divertor geometry in L-H transitions at 1.8T/1.7MA and 3.0T/2.75MA [4], no roll-over of  $P_{\text{thr}}$  was found at low density. One may speculate that  $n_{e,\text{min}}$  decreased to lower densities, which were not accessible experimentally. The physics mechanism underlying the increase in  $P_{\text{thr}}$  at low  $n_e$  has not yet been identified.

**3. L-H transitions at low density with Be/W wall.** To separate the influence of the changes in PFCs on the L-H power threshold, L-H transition experiments have been carried out in JET with the ILW with  $I_p/B_T$  and plasma shape matched to those of the MkII-HD C wall L-H discharges. The plasma density was varied from shot to shot, so as to obtain an overlap in density range with the C wall dataset. Slow input power ramps (ICRH or NBI), typically 1 MW/s, were used to measure  $P_{\text{thr}}$ .

At 1.8T/1.7MA and with C wall,  $P_{\text{thr}}$  is found to be consistent with the multi machine scaling law  $P_{\text{thr},08}$ . Conversely, in density scans with Be/W wall both  $P_{\text{thr}}$  and  $P_{\text{sep}} = P_{\text{thr}} - P_{\text{rad,bulk}}$  (the bulk radiated power) increase below a minimum density,  $n_{e,\text{min}} \sim 2.2 \times 10^{19} \text{ m}^{-3}$ , as shown in Fig. 1, thus recovering the low density behaviour first observed with MkII-GB divertor and C wall. At plasma densities above  $n_{e,\text{min}}$ ,  $P_{\text{thr}}$  is reduced by  $\sim 30\%$  and  $P_{\text{sep}}$  by  $\sim 40\%$  with Be/W wall compared to C wall. A similar, strong influence of the wall change from C to Be/W on  $P_{\text{thr}}$  and  $P_{\text{sep}}$  is also observed at 3.0T/2.75MA (Fig. 2). In addition,  $n_{e,\text{min}} \sim 3.5 \times 10^{19} \text{ m}^{-3}$  at 3.0T, having increased roughly linearly with  $B_T$  (at constant  $q_{95}$ ). This is

relevant to ITER, which needs to access the H-mode at high magnetic field ( $B_T = 5.4T$ ).

At given edge density, the L-H transition occurs at lower edge electron temperature,  $T_{e,edge}$ , with Be/W wall (Fig. 3). Due to the absence of a pedestal shape in the  $T_e$  L-mode profile up to the L-H transition,  $T_{e,edge}$  is defined as  $T_e$  (measured by fast ECE) at the radial location where the  $T_e$  pedestal is formed in H-mode. In NBI heated discharges, where  $T_{i,edge}$  can be measured with edge CXRS,  $T_{i,edge}$  and  $T_{e,edge}$  are strongly coupled over the explored density range. Together with lower  $P_{sep}$  and  $T_{e,edge}$  at the L-H transition, a weaker build-up of the density pedestal is observed after the H-mode transition, as  $P_{heat}$  slowly increased with input power ramps. We note that while  $P_{heat}$  is increased,  $P_{sep}$  remains roughly constant or increases weakly, due to the continuous rise in  $P_{rad,bulk}$ , which typically occurs at low density and low  $D_2$  fuelling. Divertor oscillations [5] are observed in the L-mode phase prior to the L-H transition, at higher density and with NBI heating. After the H-mode transition, ICRH plasmas and low density, low power NBI plasmas are quiescent, with no ELM activity. Concomitant with this, a low frequency ( $\sim 0.5-2$  kHz), axisymmetric magnetic oscillation, magnetically compatible with up/down plasma motion, is detected in many edge fluctuation diagnostics (such as Mirnov coils, fast ECE in the edge gradient region, fast IR camera data at the divertor target). As density and NBI power are increased, the MHD mode is replaced by ELM activity.

In the ILW, the sharp increase in  $P_{thr}$  for  $n_e < n_{e,min}$  in ICRH heated discharges (Fig. 1, left) is due to the strong increase in  $P_{rad,bulk}$  at low density (Fig. 4), whereas not much difference is observed in  $P_{sep}$  between NBI and ICRH discharges (Fig. 1 right). Compared to discharges with the C wall at similar densities, a lower X-point and divertor radiation is observed at the L-H transition with ILW, especially at low density (both with NBI and ICRH heating), see Fig. 3. This is consistent with the strong reduction in C concentration ( $\sim$  factor of 10) [6] in the ILW and the absence of chemical sputtering for Be. The core radiation, normalized to  $P_{loss}$  at the L-H transition, is rather similar in C and ILW for NBI heated discharges, but higher with ICRH heating over the explored density range (Fig. 4). W and Ni are the main core radiators, as measured by XUV spectroscopy, with W contributing to  $\sim 80\%$  of  $P_{rad,bulk}$ . Both W and Ni concentrations increase strongly with decreasing density and in either case higher concentrations are found in ICRH than in NBI heated discharges. The W concentration, measured from the quasi-continuum spectrum at 5 nm [7], increases from  $1.0 \times 10^{-5}$  at  $n_e = 3 \times 10^{19} \text{ m}^{-3}$  to  $1-2 \times 10^{-4}$  at  $n_e = 1.5 \times 10^{19} \text{ m}^{-3}$  with ICRH heating.

**3. Influence of divertor geometry and plasma shape on L-H threshold with ILW.** The sensitivity of  $P_{sep}$  to variations in divertor configuration and main plasma shape, which are known hidden parameters, yet not included in  $P_{thr,08}$ , has also been investigated with the ILW, by decoupling variations in lower ( $\delta_L$ ) and upper ( $\delta_U$ ) triangularity, which are taken as their proxy. At  $B_T/I_P = 2.4T/2.0MA$  and  $n_e = n_{e,min}$ ,  $P_{sep}$  is found to decrease linearly with increasing  $\delta_L$  and to increase by  $\sim 25\%$  as  $\delta_U$  is raised from  $\sim 0.19$  to  $\sim 0.38$ . Low density scans performed in the low  $\delta$  shapes revealed that, depending on the divertor configuration ( $\delta_L$ ),  $P_{thr}$  can be up to a factor 2 lower than  $P_{thr,08}$  for  $n_e > n_{e,min}$ , as shown in Fig. 5. These results point to the possible role of divertor neutral recycling and scrape-off-layer (SOL) physics in the L-H transition.

**4. Comparison with Fundamenski's L-H transition model.** The JET C and ILW L-H datasets are compared to a new model for the L-H transition [8]. The model is based on the assumption that the L-H transition occurs when edge plasma turbulence and shear Alfvén waves 'compete' near the separatrix. A local scaling for  $P_{sep}$  is derived, suggesting a critical role played by the upstream separatrix temperature  $T_{e,sep}$  at the L-H transition (eq. 16 in ref. [8]). To test this prediction against the JET L-H datasets, in particular with respect to the

observed density dependence and variations with  $B_T$ , divertor geometry and changes in PFCs, edge kinetic profiles have been collected:  $n_e$  is obtained from HRTS and Li-beam,  $T_e$  from HRTS and fast ECE profiles and  $T_i$  from edge CXRS. The model assumes  $T_i = T_e$ , which is valid for the JET dataset in the near-pedestal region, but not likely near the LCFS. A stringent test of the model requires measurement of  $T_e$  and  $n_e$  at the separatrix with an accuracy which is beyond the available diagnostic capabilities, including uncertainties associated with the determination of the EFIT separatrix position. From the comparison of the experimental data with eq. 16 of [8] we find that whereas the model captures the absolute values of  $P_{sep}$  (Fig. 6), a detailed comparison is inconclusive, due to the large uncertainties in  $T_{e,sep}$  measurements and the absence of SOL radiation fraction in the model. In particular, Fig. 6 shows that the model predicts a lower  $P_{sep}$  with C wall than with ILW, which is the opposite than what found experimentally (Fig. 1). On the other hand, inclusion of SOL physics in the model yields e.g. scalings for  $n_{e,min}$  and the minimum H-mode access power,  $P_{sep,min}$ , with  $B_T$ :  $n_{e,min} \sim B_T^{5/4}$  (eq. 39 of [8]) and  $P_{sep,min} \sim B_T^{7/5}$  (eq. 37 of [8]), which can be tested. In both cases the model captures the variation with  $B_T$  observed in JET with Be/W wall, as shown in Fig. 7 for  $n_{e,min}$  vs  $B_T$ .

### Acknowledgments

This work was supported by EURATOM and carried out within the framework of the European Fusion Development Agreement. The views and opinions expressed herein do not necessarily reflect those of the European Commission.

### References

- [1] Y. Martin et al., JPCS **123** (2008) 012033.
- [2] L.D. Horton et al., 26<sup>th</sup> EPS Conf. on Controlled Fusion and Plasma Physics (Maastricht) 1999.
- [3] Y. Andrew et al., Plasma Phys. Control. Fusion, **48** (2006) 479.
- [4] C.F. Maggi et al., 38th EPS Conf. on Plasma Physics (Strasbourg) 2011.
- [5] A. Loarte et al., Phys. Rev. Lett. **83** (1999) 3657.
- [6] S. Brezinsek et al., 20<sup>th</sup> International Conf. on PSI, Aachen 2012, submitted to JNM.
- [7] T. Pütterich et al., Plasma Phys. Control. Fusion **50** (2008) 085016.
- [8] W. Fundamenski et al., Nucl. Fusion **52** (2012) 062003.

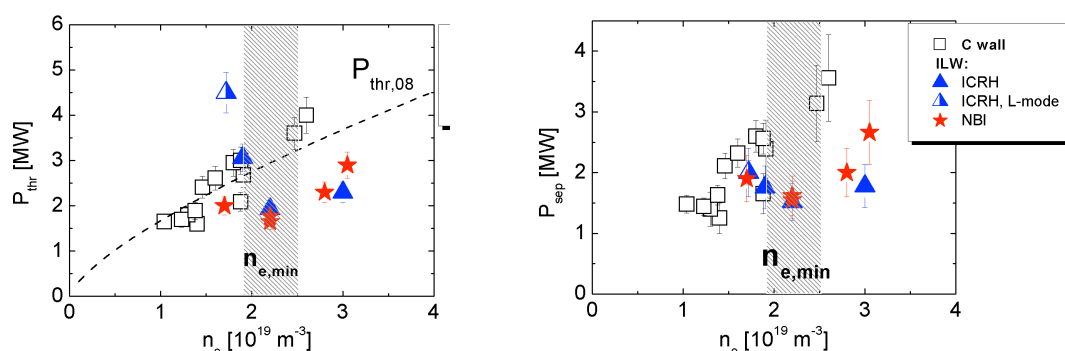
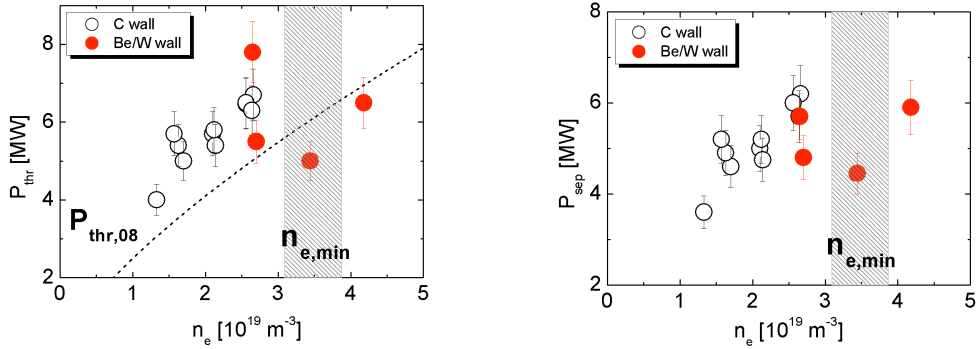
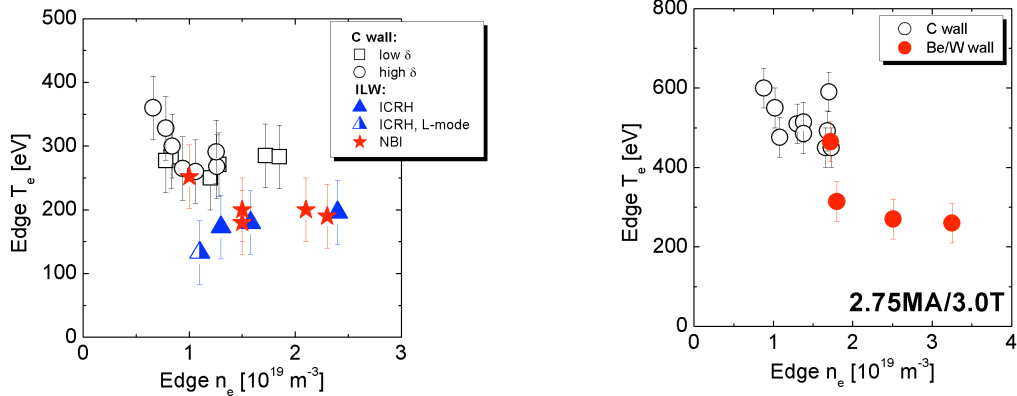


Figure 1. From left to right:  $P_{thr}$  and  $P_{sep}$  at 1.8T/1.7MA for C and Be/W wall datasets.



**Figure 2.** From left to right:  $P_{thr}$  and  $P_{sep}$  at 3.0T/2.75MA for C and Be/W wall datasets.



**Figure 3.** Edge  $T_e$  vs edge  $n_e$  at the L-H transition for C and Be/W wall: at 1.8T (left) and 3.0T (right).

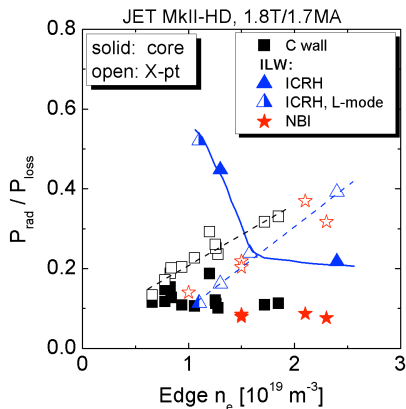


**Figure 4.** Radiated power, normalized to  $P_{loss}$ , at the L-H transition for C and Be/W wall (1.8T/1.7MA).

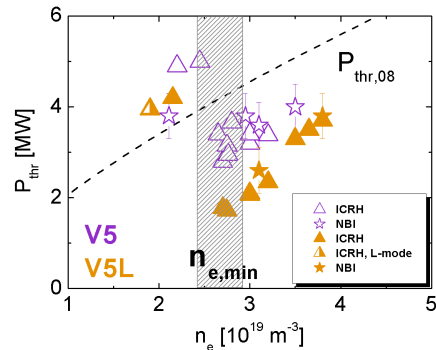


**Figure 5.** Variation of  $P_{thr}$  vs  $n_e$  with Be/W wall (2.4T/2.0MA) at low  $\delta$  for two divertor configurations with different strike point positions.

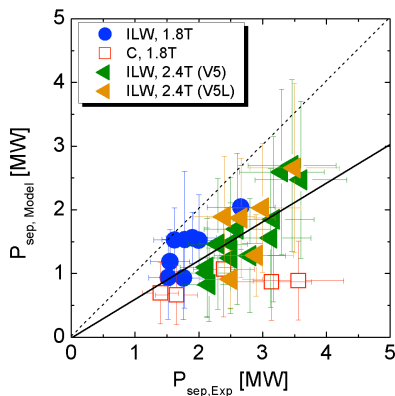


**Figure 6.** Predicted vs measured  $P_{sep}$ .

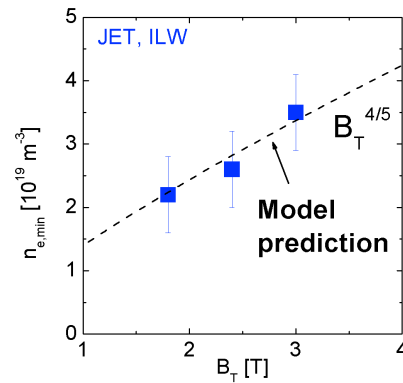


**Figure 7.**  $n_{e,min}$  variation vs  $B_T$  in JET with ILW.